
Dependency-Aware Parallel Decoding via Attention for Diffusion LLMs

Bumjun Kim^{*1} Dongjae Jeon^{*2} Moongyu Jeon¹ Albert No¹

Abstract

Parallel decoding for diffusion LLMs (dLLMs) is difficult because each denoising step provides only token-wise marginal distributions, while unmasking multiple tokens simultaneously requires accounting for inter-token dependencies. We propose **Dependency-Aware Parallel Decoding (DAPD)**, a simple, training-free decoding method that uses self-attention to induce a conditional dependency graph over masked tokens. At each iteration, edges in this graph capture strong token interactions, while non-edges indicate weak dependence. Parallel decoding is then reduced to selecting an independent set on the graph and unmasking the selected tokens in parallel. This avoids co-updating strongly coupled tokens without auxiliary models or retraining. Experiments on LLaDA and Dream show that DAPD improves the accuracy–steps trade-off over existing methods and enables more globally distributed parallel updates that better exploit the any-order generation capability of dLLMs.

1. Introduction

Diffusion models have achieved remarkable success in continuous domains such as image and audio generation (Sohl-Dickstein et al., 2015; Song & Ermon, 2019; Ho et al., 2020; Song et al., 2021), and have recently been extended to discrete data (Hoogeboom et al., 2021; Austin et al., 2021a; Campbell et al., 2022; Lou et al., 2024). In particular, Masked Diffusion Models (MDMs) (Sahoo et al., 2024; Shi et al., 2024; Ou et al., 2025) have emerged as a promising alternative to autoregressive (AR) models (Radford et al., 2018; 2019). With large-scale models such as LLaDA (Nie et al., 2025) and Dream (Ye et al., 2025), masked diffusion-based LLMs (dLLMs) demonstrate strong scalability and competitive language modeling performance.

Parallel decoding, the ability to generate multiple tokens

^{*}Equal contribution ¹Department of Artificial Intelligence, Yonsei University ²Department of Computer Science, Yonsei University. Correspondence to: Albert No <albertno@yonsei.ac.kr>.

simultaneously, is often highlighted as a key advantage of dLLMs (Nie et al., 2025; Ye et al., 2025), offering the potential to significantly reduce inference latency compared to the serial nature of AR generation. However, realizing this potential is challenging: dLLMs are typically trained to model only token-wise conditional marginals at masked positions, and marginals alone do not determine the true joint distribution. Consequently, independently sampling multiple tokens from these marginals ignores their inter-dependencies, leading to *joint-marginal mismatch* and often producing outputs that are locally plausible yet globally inconsistent (Ben-Hamu et al., 2025; Wu et al., 2025).

Existing training-free parallel decoding strategies (Wu et al., 2025; Ben-Hamu et al., 2025; Kim et al., 2025c) often sidestep joint dependencies by relying on marginal-based signals such as confidence scores (Chang et al., 2022; Kim et al., 2025b). While such methods filter out uncertain tokens, they do not account for interactions between masked positions, leaving the joint-marginal mismatch unresolved when multiple confident yet dependent tokens are decoded in parallel. Parallel decoding methods with additional training or auxiliary planners have also been explored (Israel et al., 2025; Bao et al., 2025; Chen et al., 2025), but they often incur extra complexity or rely on surrogate objectives.

In this work, we aim to capture joint dependencies to address the joint-marginal mismatch, utilizing the model’s self-attention as a proxy for conditional independence. Building on this insight, we model the interactions among masked tokens as a *Markov Random Field (MRF)*. We use attention to estimate token dependencies and represent them as a graph, where edges denote significant interactions. We empirically validate this representation through controlled experiments on synthetic data, confirming that attention signals reliably capture the ground-truth interaction structure. This graph serves as a structural guide for identifying which tokens can be safely decoded in parallel.

We then cast parallel decoding through the lens of graph coloring, a classical abstraction for scheduling mutually conflicting items: given a graph where edges connect pairs that should not be processed together, each color class corresponds to an independent set that can be handled in parallel. Under this view, parallel decoding in dLLMs becomes a dynamic coloring problem, where masked tokens are nodes



Figure 1. Visualization of unmasking trajectories for DAPD (ours) and Fast-dLLM during the initial 50% of decoding steps. While DAPD processes independent questions simultaneously to maximize global parallelism, Fast-dLLM exhibits a highly sequential unmasking pattern. Other baselines demonstrate similar sequential behaviors (see App. D). Detailed discussion is provided in Sec. 6.

and attention-induced couplings define edges. Selecting a set of tokens to unmask in parallel thus reduces to choosing an (approximately) independent set on the current graph, which serves as a linguistically motivated relaxation of joint independence and helps mitigate joint–marginal mismatch. We implement this idea using a Welsh–Powell-inspired heuristic (Welsh & Powell, 1967) that prioritizes high-degree “hub” tokens, simplifying the residual graph across decoding steps. Across benchmarks on LLaDA (Nie et al., 2025) and Dream (Ye et al., 2025), **DAPD** consistently achieves a better accuracy–steps trade-off than state-of-the-art baselines.

DAPD is training-free, relying only on model-internal signals available at inference time to guide parallel unmasking, without any additional training cost or auxiliary models. Beyond this simplicity, we observe a qualitative difference in the resulting decoding dynamics. Baseline strategies driven primarily by marginal confidence tend to unmask tokens in contiguous clusters, effectively behaving like two-sided autoregressive decoding that expands inward from the sequence boundaries and underutilizes global context. In contrast, DAPD generates tokens in a spatially dispersed manner, prioritizing independent regions across the entire sequence before filling in the gaps. This highlights a key advantage of discrete diffusion: leveraging bidirectional context for non-sequential, global generation, and suggests global parallelism as a natural decoding paradigm for dLLMs.

2. Preliminaries

2.1. Masked Diffusion Models

In Masked Diffusion Models (MDMs), the diffusion process is implemented through progressive token masking. Specifically, a subset of tokens in a sequence $\mathbf{x} = x^1 \dots x^L \in \mathcal{V}^L$ is replaced with a special mask token $[\mathbf{M}]$, and the model learns to recover the original tokens (Austin et al., 2021a;

Lou et al., 2024). For a uniformly selected time $t \in [0, 1]$, each token in the original sequence $\mathbf{x}_0 = x_0^1 \dots x_0^L$ is independently masked with probability t to produce a corrupted sequence \mathbf{x}_t . The model is trained to predict the original token at each masked position by learning the conditional probability $p_\theta(x_0^i | \mathbf{x}_t)$, using the following weighted cross-entropy loss. This loss serves as a variational upper bound on the negative log-likelihood $-\log p_\theta(\mathbf{x}_0)$ (Sahoo et al., 2024; Shi et al., 2024; Ou et al., 2025):

$$\mathcal{L}_{\text{MDM}}(\mathbf{x}_0; \theta) = -\mathbb{E}_{t, \mathbf{x}_t} \left[\frac{1}{t} \sum_{i: x_t^i = [\mathbf{M}]} \log p_\theta(x_0^i | \mathbf{x}_t) \right].$$

After training, the model provides token-wise conditional distributions $p_\theta(x^i | \mathbf{x})$ for all positions $i \in \{1, \dots, L\}$ and masked sequences $\mathbf{x} \in \overline{\mathcal{V}}^L$, where $\overline{\mathcal{V}} = \mathcal{V} \cup \{[\mathbf{M}]\}$. These conditionals generate a full sequence \mathbf{x}_0 by iteratively unmasking tokens from the fully masked input $\mathbf{x}_1 = [\mathbf{M}] \dots [\mathbf{M}]$. According to the factorization

$$p(\mathbf{x}_0) = \prod_{i=1}^L p(x^{\pi(i)} | \mathbf{x}^{\pi(<i)}),$$

unmasking the sequence according to any permutation π on $\{1, \dots, L\}$ theoretically yields samples from the same distribution. In practice, however, the choice of unmasking order is known to have a significant impact on generation quality (Zheng et al., 2024; Kim et al., 2025b). A common and effective strategy is confidence-based sampling (Chang et al., 2022), which prioritizes the masked position whose predictive distribution has the largest maximum probability. Intuitively, by unmasking tokens with the lowest uncertainty first, this approach prevents error propagation and ensures that subsequent predictions rely on a trustworthy context.

More recently, many MDM variants have adopted a semi-autoregressive block generation scheme (Arriola et al., 2025;

Wu et al., 2025), in which a sequence is partitioned into fixed-length blocks. Within each block, tokens are generated using diffusion, while blocks are processed sequentially in a left-to-right order. This formulation leverages the inherent left-to-right dependency of natural language across blocks and enables block-level KV caching during inference.

Recent work has shown that MDMs can be successfully scaled to large language models, giving rise to Diffusion Large Language Models (dLLMs) (Khanna et al., 2025). These include models trained either from scratch or via autoregressive initialization, such as LLaDA (Nie et al., 2025) and Dream (Ye et al., 2025).

2.2. Parallel Decoding of dLLMs

Challenge of Parallel Decoding. Parallel decoding is often highlighted as a key advantage of dLLMs, allowing multiple tokens to be generated simultaneously at each denoising step. The computational cost of dLLMs is dominated by the number of model forward passes, often referred to as function evaluations (NFE). Since each decoding step requires exactly one forward pass to update the sequence, the total NFE is equivalent to the number of decoding steps. Thus, minimizing the step count is crucial for efficiency. By unmasking multiple tokens within a single step, parallel decoding can significantly reduce this cost.

However, dLLMs are trained to model conditional marginal distributions at each masked position. As a result, unmasking multiple tokens simultaneously can yield errors due to mismatch between the true joint distribution and the product of marginals (Ben-Hamu et al., 2025; Wu et al., 2025):

$$p(x^{i_1}, \dots, x^{i_k} | \mathbf{x}) \neq \prod_{j=1}^k p(x^{i_j} | \mathbf{x}). \quad (1)$$

When multiple tokens are decoded in parallel, this discrepancy can accumulate, as dependencies among the tokens are not fully accounted for.

As an illustrative example, consider the prompt “The capital of [M] is [M]” (Song & Zhou, 2025). The model may assign a high marginal probability to “France” at the first position and to “London” at the second. Although each prediction is plausible in isolation, sampling both positions simultaneously can yield an inconsistent pair, illustrating that ignoring dependencies between masked positions can lead to globally invalid outputs.

Training-free parallel decoding for dLLMs. As discussed above, a central difficulty of parallel unmasking in dLLMs is the *joint-marginal mismatch* (Eq. (1)), which arises when masked positions are interdependent. Most training-free samplers therefore focus on designing criteria to select positions that can be safely decoded together,

typically using marginal signals available at inference time.

We consider several representative training-free strategies as baselines. The most direct approach ranks masked positions by marginal confidence and decodes the top- k ranked positions in parallel (Nie et al., 2025). **EB-Sampler** (Ben-Hamu et al., 2025) instead selects the subset of positions that satisfies an entropy-based bound, aiming to control the risk of decoding dependent tokens together. **Fast-dLLM** (Wu et al., 2025) applies selective parallelism by unmasking only positions whose confidence exceeds a fixed threshold. **KLASS** (Kim et al., 2025c) further augments confidence with a stability signal defined by the token-wise KL divergence between consecutive denoising steps, and parallel-unmasks tokens that are both confident and stable.

Beyond the above training-free methods, there exist parallel decoding approaches that rely on additional training, auxiliary models, or modified strategies (Israel et al., 2025; Bao et al., 2025; Chen et al., 2025), which we do not pursue here. These methods handle inter-token coupling more explicitly, but incur extra cost and may depart from the ELBO-based formulation via surrogate objectives, auxiliary targets, or training-inference mismatches.

3. Modeling Dependencies via Graphs

Departing from existing marginal-based strategies that neglect cross-position interactions (Sec. 2.2), we introduce a method that leverages the model’s internal self-attention mechanism to capture the dependency structure of the masked tokens. We formulate this structure as a *Markov Random Field (MRF)*, where the attention mechanism defines the conditional independence properties between variables. Within this probabilistic framework, we reduce parallel decoding to selecting an independent set of the induced MRF.

3.1. Attention-Induced Markov Random Fields

We model the interactions among masked positions at each step t as an MRF, which explicitly characterizes the conditional independence structure of the masked tokens.

Definition 3.1 (Markov Random Field). A collection of random variables $X = \{X_v\}_{v \in V}$ constitutes a *Markov Random Field (MRF)* with respect to an undirected graph $G = (V, E)$ if it satisfies the *pairwise Markov property*: for any two non-adjacent nodes $u, v \in V$ (i.e., $(u, v) \notin E$), the variables X_u and X_v are conditionally independent given all other variables $X_{V \setminus \{u, v\}}$.

Remark 3.2. Another common way to define an MRF is via a clique-factorized form. Under positivity (i.e., $p(x) > 0$ for all x), this definition is equivalent to the pairwise Markov property with respect to G (Koller & Friedman, 2009).

Intuitively, the absence of an edge means that, once the

global context is given, the two variables no longer provide information about each other.

Graph Construction in dLLM Decoding. We construct an MRF induced by a pretrained dLLM. At each decoding step, masked positions can be viewed as random variables, and our goal is to characterize their dependencies by constructing the corresponding MRF graph. We use attention to define the edge structure, treating stronger attention as indicating a stronger dependency.

Let $V_t = \{i \in \{1, \dots, L\} : x_t^i = [\mathbf{M}]\}$ denote the set of masked indices at step t . We construct a graph $G_t = (V_t, E_t)$, where the edge set E_t is determined using the model’s self-attention maps. More precisely, we define a symmetric *edge score* s_{ij} to quantify the interaction strength between positions i and j :

$$s_{ij} := \frac{1}{2}(a_{ij} + a_{ji}),$$

where a_{ij} represents the attention weight from i to j (the choice of layer and head is specified in Secs. 3.2 and 4.3). We interpret the magnitude of this score as a proxy for the strength of conditional dependence, thereby aligning this structure with the edge set E_t .

Using a threshold $\tau_t \geq 0$, we establish the edges as follows:

$$(i, j) \in E_t \iff s_{ij} > \tau_t.$$

Under this construction, an edge ($s_{ij} > \tau_t$) represents a considerable dependency, while a non-edge ($s_{ij} \leq \tau_t$) indicates that the interaction is negligible.

Justification: Attention as Conditional Independence.

We justify our attention-based edge construction by relating low attention to conditional independence. In a Transformer, negligible attention between positions i and j indicates that the model places little weight on the representation at j when forming the contextualized representation used to predict the token at i . As a result, once we condition on the remaining context $X_{V_t \setminus \{i, j\}}$, the model’s predictive distribution for X_i becomes effectively invariant to whether X_j is revealed. This intuition is captured by the approximation

$$p_\theta(X_i | X_{V_t \setminus \{i\}}) \approx p_\theta(X_i | X_{V_t \setminus \{i, j\}}),$$

Namely, X_i and X_j are approximately conditionally independent given the remaining variables $X_{V_t \setminus \{i, j\}}$. Therefore, defining non-edges via low attention is consistent with the local Markov property underlying MRFs.

3.2. Validation of Graph Construction

We empirically validate our MRF construction in a controlled toy setting to verify whether attention signals can

effectively capture the underlying conditional independence structure and distinguish between graph edges. Experimental details are provided in App. A.

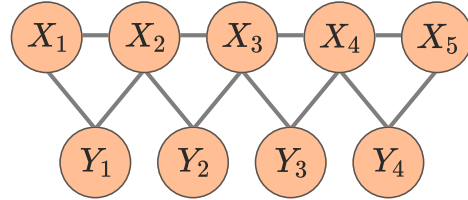


Figure 2. Illustration of synthetic MRF dataset.

Setup. We train simple masked diffusion models (MDMs; RADD; Ou et al. (2025)) on a synthetic dataset composed of length-9 sequences $(X_1, \dots, X_5, Y_1, \dots, Y_4)$. The variables (X_1, \dots, X_5) are sampled independently from the discrete uniform distribution on $\{0, 1, 2\}$, and the remaining tokens are deterministically defined by

$$Y_i := (X_i + X_{i+1}) \bmod 3, \quad i = 1, 2, 3, 4.$$

This construction induces four local constraints, each involving the triple (X_i, X_{i+1}, Y_i) . Accordingly, we represent the ground-truth MRF structure as the union of four triangles:

$$\{X_i, X_{i+1}, Y_i\}, \quad i = 1, 2, 3, 4.$$

Although X_i and X_{i+1} are marginally independent, the constraint $Y_i \equiv X_i + X_{i+1}$ induces conditional dependence given Y_i , necessitating a fully connected triangle for each triple. Thus, as shown in Fig. 2, the ground-truth MRF consists exclusively of four triangles, with no connections between variables not involved in a common constraint.

Edge Detection		Degree Estimation
AUC	Ratio (Edge / Non-Edge)	OVR
0.928	2.204	0.04

Table 1. Metrics for edge detection (AUC and edge-to-non-edge score ratio) and degree estimation (OVR). Results are averaged over 100 random sampling paths and across all decoding steps. Comprehensive step-wise results are provided in App. A.

Edge Score. For each pair of positions (i, j) , we compute the edge score s_{ij} by averaging the attention weights over all heads and the top two layers of the Transformer out of eight. We focus on upper layers because they tend to integrate information propagated across the network, capturing more global dependencies, whereas lower layers are often dominated by local token-level processing (Tenney et al., 2019a;b; Jawahar et al., 2019).

Separability of edges and non-edges. We first evaluate whether the attention-based score s_{ij} can distinguish ground-truth edges in the MRF from non-edges. We compare the empirical distributions of s_{ij} for the two groups and report

(i) the area under the ROC curve (AUC) for edge classification using s_{ij} and (ii) the ratio of their mean scores. Across multiple runs, s_{ij} exhibits clear separation between edges and non-edges, achieving AUC of 0.928 and edge-to-non-edge score ratio of 2.204 (Tab. 1). These results suggest that attention provides a reliable signal for recovering the underlying MRF structure.

Degree estimation from attention sums. While the interaction score s_{ij} provides strong separability, choosing an exact threshold τ_t to recover the exact edge set remains challenging. However, our proposed algorithm (Sec. 4) relies primarily on *sorting* nodes by degree, rather than on estimating the exact edge set. Consequently, we focus on validating whether simple attention aggregates can serve as a robust proxy for the true node degree in the ground-truth MRF. We examine whether the sum of edge scores

$$\tilde{d}_i := \sum_{j \in V_i \setminus \{i\}} s_{ij}$$

aligns with the true degree d_i of node i . We introduce an intuitive measure, the *Order Violation Rate* (OVR), defined as the fraction of pairs whose strict order under the true degrees is reversed by the proxy scores. Formally,

$$\text{OVR}(t) = \frac{1}{\binom{|V_t|}{2}} \sum_{d_i < d_j} \mathbb{1}[\tilde{d}_i > \tilde{d}_j],$$

Lower OVR indicates better agreement with the true ordering. We find that the ordering is highly consistent (mean OVR = 0.04; Tab. 1), suggesting that the proxy \tilde{d}_i provides a reliable estimate for node degree, and thus for the relative structural importance of the corresponding variable.

4. Dependency-Aware Parallel Decoding

In Sec. 3, we established that the interactions among masked tokens can be modeled as a Markov Random Field (MRF), denoted as G_t . We now leverage this structural understanding to guide parallel decoding. At each decoding step, our goal is to select a subset of masked tokens that are approximately conditionally independent given the context, thereby reducing joint-marginal mismatch and enabling parallel generation that better matches the true joint distribution. By maximizing the size of such a valid subset that satisfies these dependency constraints, we aim to effectively reduce the total number of decoding steps (NFE), the primary computational bottleneck identified in Sec. 2.2, without compromising generation quality.

4.1. Independent Set Selection via Structural Relaxation

To determine the set of tokens to unmask at step t , we select an *independent set* $S \subseteq V_t$, defined as a subset of nodes with

no direct edges between them. Theoretically, a sufficient condition for full joint independence in an MRF is that the nodes are pairwise disconnected (i.e., no path exists between any pair in S) rather than merely non-adjacent (Koller & Friedman, 2009). However, we adopt pairwise non-adjacency as a sufficient condition for practical decoding. Enforcing strict separation incurs high computational overhead for verification and results in prohibitively small batches, severely limiting parallel speedup. Furthermore, in natural language, dependencies are predominantly captured by direct interactions; instances of joint dependence arising solely from indirect paths are negligible. Thus, this structural relaxation effectively mitigates the risk of severe incoherence while maximizing decoding efficiency.

4.2. Parallel Decoding as Dynamic Graph Coloring

Given the MRF constructed above, parallel decoding reduces to the problem of selecting independent sets in the graph. In dLLM decoding, our objective is to minimize the number of decoding steps, which is equivalent to covering all masked positions with as few independent sets as possible. This directly maps the problem to *graph coloring*: in a graph, a proper coloring partitions nodes into disjoint independent sets (color classes), and the minimum number of colors required (the chromatic number) corresponds to the minimum number of parallel decoding steps.

While classical graph coloring is defined on a static graph, our setting differs in that the MRF $G_t = (V_t, E_t)$ is dynamic. After each decoding step, the set of masked nodes V_t shrinks and the edge structure E_t is perturbed as new context becomes available. Nevertheless, the core combinatorial intuition remains applicable. At each step, selecting an independent set can be viewed as a coloring of the current graph, with the goal of minimizing the total number of decoding steps over time. This motivates us to adopt graph-coloring-inspired strategies for parallel decoding.

4.3. Implementation via a Coloring Strategy

We now operationalize the graph-coloring perspective by designing a sequential independent-set selection procedure. A natural greedy objective is to maximize the number of nodes decoded at each step, i.e., to select a maximum independent set of the current graph. However, our goal is to minimize the total number of steps, which corresponds to covering the node set with as few independent sets (color classes) as possible. These objectives need not coincide: heuristics that favor large independent sets often prioritize low-degree nodes, whereas reducing the number of future color classes benefits from resolving high-degree nodes early.

Accordingly, we adopt the *Welsh–Powell algorithm* (Welsh & Powell, 1967), a degree-prioritized greedy coloring strategy. At each step, we order the remaining nodes by non-

increasing degree and then scan this list, adding a node whenever it is non-adjacent to the nodes already selected. This procedure constructs a maximal (not necessarily maximum) independent set to be decoded in parallel. Although the resulting set may be smaller than a maximum independent set in the current step, prioritizing high-degree nodes tends to simplify the residual graph, making it easier to cover with fewer independent sets in subsequent steps and ultimately reducing the total number of decoding steps.

Method. We instantiate this algorithm for dLLM decoding as **Dependency-Aware Parallel Decoding (DAPD)** to construct our parallel batches. At each decoding step t , we approximate the MRF $G_t = (V_t, E_t)$ using the attention-derived edge scores s_{ij} . We estimate the degree of each node $i \in V_t$ using \tilde{d}_i , and define edges by thresholding the scores with a conservative (small) τ_t . We set τ_t low so that we declare a non-edge only when the interaction is confidently negligible, prioritizing conflict avoidance in independent-set selection over edge-set precision.

Given this proxy graph, we construct an independent set S using the Welsh-Powell-motivated strategy:

1. **Ordering:** We sort all masked nodes in descending order of their proxy degree \tilde{d}_i .
2. **Greedy Selection:** We iterate through the list, adding a node to S if and only if it is non-adjacent to all nodes currently in S .
3. **Update:** All tokens in S are unmasked simultaneously. The graph is then recomputed for the next step.

From a dLLM perspective, this strategy prioritizes positions that strongly interact with many others. Resolving these “hub” nodes early effectively breaks the major dependency chains, sparsifying the graph for subsequent steps and enabling larger parallel batches later in the process.

Practical Implementation. In our final implementation, we refine the sorting metric to a confidence-weighted degree $\tilde{d}_i \cdot \text{conf}_i$, where conf_i denotes the marginal confidence at position i , the maximum predicted token probability. Since conf_i reflects the probability that the most likely token at position i will be correctly generated, multiplying \tilde{d}_i by conf_i can be interpreted as measuring the *expected effective degree* of node i . That is, while \tilde{d}_i captures the structural influence of a position in the dependency graph, $\tilde{d}_i \cdot \text{conf}_i$ quantifies how much of this influence is expected to be realized given the model’s current uncertainty. This criterion prioritizes nodes that are both structurally important and reliably predictable, aligning the ordering metric with the goal of reducing downstream conflicts in iterative decoding.

As decoding progresses and strong dependencies are resolved, the MRF becomes sparse. When the remaining mask ratio falls below 50%, we switch to a confidence-threshold rule, unmasking all positions with confidence > 0.9 (Wu et al., 2025). In graph terms, this corresponds to a regime where most remaining nodes have near-zero degree (i.e., are conditionally independent given the resolved context). In this disconnected regime, confidence-based sampling effectively serves as an aggressive independent-set approximation, enabling efficient completion. We empirically verify this sparsification behavior in Sec. 6.

5. Experiments

Setup. We evaluate DAPD on two representative open-source dLLMs: LLaDA-8B-Instruct (Nie et al., 2025) and Dream-7B-Instruct (Ye et al., 2025). We compare against training-free parallel decoding baselines, including EB-Sampler (Ben-Hamu et al., 2025), KCLASS (Kim et al., 2025c), and Fast-dLLM (Wu et al., 2025). For all baselines, we adopt a top-1 confidence-based unmasking strategy and use the best hyperparameters reported in the original papers.

Following prior work (Ben-Hamu et al., 2025; Kim et al., 2025c; Wu et al., 2025), we evaluate our method on mathematical reasoning tasks (GSM8K (Cobbe et al., 2021), Math500 (Hendrycks et al., 2021)) and code generation tasks (MBPP (Austin et al., 2021b), HumanEval (Chen et al., 2021)). To assess instruction-following capability, we additionally include IFEval (Zhou et al., 2023). All evaluations are conducted using the `lm-eval` framework (Gao et al., 2024) with a maximum generation length of 256 tokens. As a complementary evaluation focused on parallel decoding behavior, we also report results on ParallelBench (Kang et al., 2025), which is specifically designed to stress-test parallel decoding by inducing strong inter-token dependencies and exposing joint-marginal mismatch. Full experimental details and configurations are provided in App. B.

Results. We begin by evaluating training-free baselines on LLaDA under 1-block decoding; however, their accuracy collapses in this regime, making direct comparison impractical (see Tab. 4). We find that this degradation is primarily driven by premature termination due to EOS overflow (Kim et al., 2025a). To ensure a fair evaluation, we follow the protocols established in the official LLaDA implementation (Nie et al., 2025), applying block-wise decoding and EOS suppression to the baselines. In contrast, our method is evaluated using a single block by default, highlighting its robustness under single-block parallel decoding.

Fig. 3 demonstrates the performance of various decoding strategies across the accuracy–steps trade-off. Notably, our method consistently occupies the upper-left region. In particular, on MBPP and IFEval, DAPD attains significantly

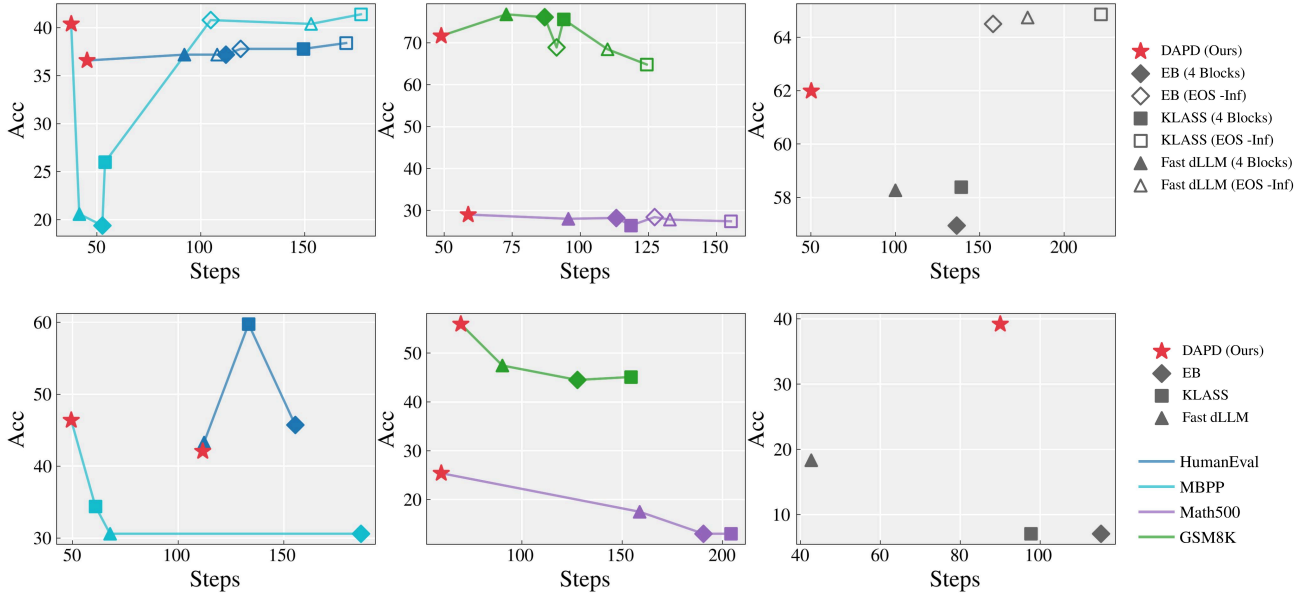


Figure 3. Accuracy–Steps trade-off of decoding strategies on two dLLMs. **Top:** LLaDA. **Bottom:** Dream. **Left:** code tasks (HumanEval, MBPP). **Middle:** math tasks (GSM8K, Math500). **Right:** instruction-following task (IFEval). Markers denote decoding strategies. For LLaDA, baselines are shown with block decoding and EOS suppression settings (“4 Blocks” and “EOS-Inf”), while DAPD is evaluated in the single-block regime by default. For Dream, all methods are evaluated in the single-block regime. Colored lines indicate different tasks.

higher accuracy than block-wise baselines. Although single-block decoding with EOS suppression achieves comparable accuracy, it requires significantly more decoding steps. On the remaining tasks, DAPD achieves comparable accuracy while providing substantial speedups over other methods. Additionally, as shown in Fig. 4, our method achieves a more favorable score–steps trade-off than the baselines on most ParallelBench tasks. This indicates that our approach more effectively identifies and updates low-dependency token sets in parallel, even under complex dependency structures.

Unlike LLaDA, Dream does not support block-wise decoding or EOS suppression in its official implementation. Moreover, we observe that Dream does not exhibit severe EOS overflow at a generation length of 256 tokens. Accordingly, we evaluate all methods under a unified single-block decoding setup. As shown in Fig. 3, our method maintains a superior accuracy–steps trade-off relative to the baselines. This trend aligns with our findings on LLaDA, suggesting that our approach generalizes across diverse dLLMs.

6. Analysis of Decoding Behavior

In this section, we examine the token unmasking dynamics of different decoding strategies. Ideally, an optimal parallel decoding should identify and exploit conditionally independent subsets of tokens under the current context, enabling them to be decoded simultaneously and thus maximizing computational throughput. However, such independence is difficult to isolate in standard benchmarks, which typically

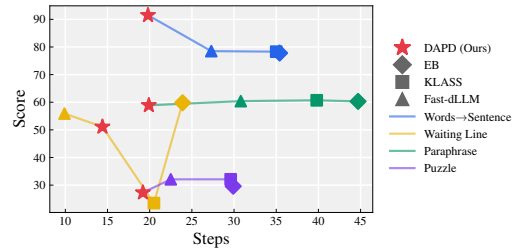


Figure 4. Score–Steps trade-off of different decoding strategies on ParallelBench using LLaDA. Colors denote different tasks.

evaluate generation quality on a single globally coherent answer, thereby inducing strong semantic and statistical coupling across tokens.

Setup. With this in mind, we turn to a setting where conditional independence naturally arises: prompts that bundle multiple independent queries into a single generation. Specifically, we draw samples from TriviaQA (Joshi et al., 2017), a fact-oriented benchmark characterized by concise and unambiguous answers. We aggregate five randomly sampled questions into a single prompt, resulting in a total of 500 evaluation samples (2,500 individual questions).

All methods are evaluated on LLaDA with a maximum generation budget of 256 tokens. To isolate the effects of the decoding strategies, we disable block-wise decoding. We do not observe EOS overflow here, as the input prompts are sufficiently short. Details regarding dataset construction and the broader experimental setup are provided in App. C.

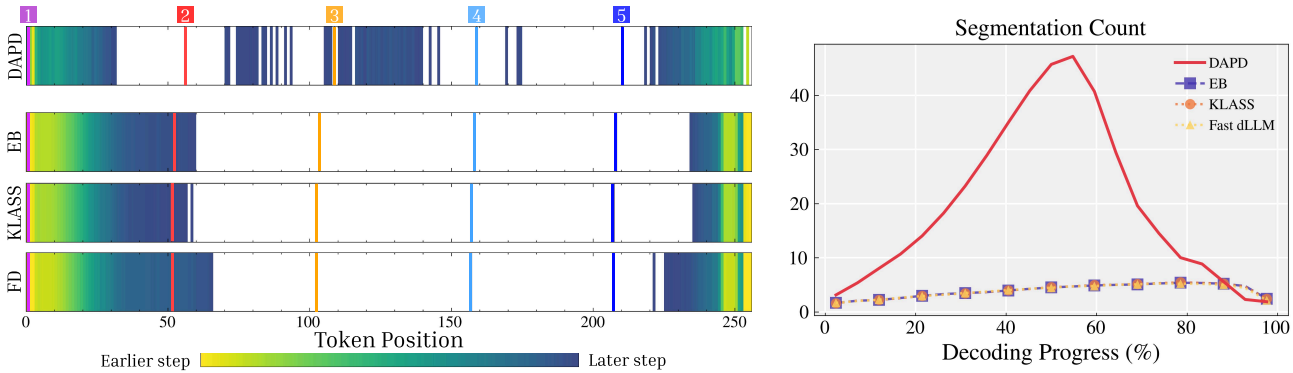


Figure 5. **Left:** Distribution of tokens unmasked during the initial 40% of decoding. Progress is normalized by total steps per sample and method. Heatmaps show the average unmasking trajectory, where lighter colors indicate earlier unmasking and white regions denote tokens remaining masked. Vertical color bars (labeled above) indicate average starting positions for the five questions; FD denotes Fast-dLLM. **Right:** Average number of isolated segments per decoding step, characterizing sequence fragmentation. Notably, DAPD exhibits a distinct unmasking pattern, whereas baselines show highly similar behaviors.

Method	Acc.	Steps (Speed Up)
Original	52.64	256.0
Fast-dLLM	52.12	124.4 (2.06×)
KLASS	52.2	177.4 (1.44×)
EB	51.2	131.3 (1.95×)
DAPD (Ours)	52.08	66.2 (3.87×)

Table 2. Accuracy and average decoding steps, with relative speedup measured against step-by-step LLaDA decoding strategy (referred to as Original in the table).

Results. Fig. 5 and Tab. 2 summarize the qualitative and quantitative behaviors induced by different decoding strategies. Fig. 5 (left) shows that DAPD exhibits a qualitatively distinct decoding pattern compared to baselines that rely on marginal confidence, while Fig. 5 (right) reports the corresponding evolution of the *segment count*, defined as the number of disjoint contiguous segments of unmasked tokens in the generation region at each step. DAPD follows a characteristic trajectory in which the segment count increases toward the midpoint of generation and then drops sharply as segments merge. In contrast, baseline methods maintain only a small number of segments throughout decoding. These structural differences directly translate into efficiency gains. As shown in Tab. 2, DAPD matches the accuracy of LLaDA with step-by-step decoding while significantly reducing the number of generation steps, achieving more than 1.8× speedup over competing strategies and a 3.8× speedup compared to standard step-by-step decoding by solving independent questions concurrently.

Sequential bottlenecks in baselines. Fig. 5 indicates that baseline methods exhibit highly localized decoding trajectories. Despite the independence of the queries, these approaches predominantly unmask adjacent tokens, progressively focusing on contiguous regions and resolving queries sequentially. As a result, the segment count remains low, reflecting an autoregressive-like behavior constrained by spatial locality. This highlights a key limitation of relying

solely on marginal confidence as a decoding critic: marginal scores are heavily influenced by local context and fail to promote concurrent generation across distant regions. Consequently, baseline methods are unable to fully exploit the throughput benefits of parallel decoding or the any-order flexibility that dLLMs are designed to support.

Spatially dispersed generation in DAPD. In contrast, DAPD encourages a spatially dispersed, largely order-agnostic unmasking behavior across the five independent queries from early decoding stages. By explicitly accounting for inter-token dependencies, DAPD avoids committing to a single contiguous region and instead distributes unmasking decisions across distant positions. This dispersed behavior leads to the formation of multiple disjoint segments early in generation, as reflected by the rise in segment count. Importantly, early spatially dispersed unmasking provides partial context across all queries, which subsequently reduces uncertainty when filling the remaining masked spans and enables rapid consolidation in later steps. Taken together, this behavior more faithfully realizes the core promise of dLLMs: leveraging bidirectional context to support truly any-order generation, rather than collapsing into an autoregressive-like trajectory.

7. Conclusion

We propose Dependency-Aware Parallel Decoding (DAPD) for dLLMs, a training-free method that leverages self-attention to account for inter-token dependencies beyond marginal confidence. DAPD builds an attention-induced Markov Random Field at each step, estimates node degrees from attention aggregates, and selects an independent set via a greedy scheduler. Across LLaDA and Dream, DAPD improves the accuracy–steps trade-off over strong training-free baselines and shifts decoding from locally clustered behavior to globally dispersed, order-flexible generation.

Impact Statement

This paper presents work whose goal is to advance the field of machine learning. There are many potential societal consequences of our work, none of which we feel must be specifically highlighted here.

References

- Arriola, M., Gokaslan, A., Chiu, J. T., Yang, Z., Qi, Z., Han, J., Sahoo, S. S., and Kuleshov, V. Block diffusion: Interpolating between autoregressive and diffusion language models. In *ICLR*, 2025.
- Austin, J., Johnson, D. D., Ho, J., Tarlow, D., and Van Den Berg, R. Structured denoising diffusion models in discrete state-spaces. In *NeurIPS*, 2021a.
- Austin, J., Odena, A., Nye, M., Bosma, M., Michalewski, H., Dohan, D., Jiang, E., Cai, C., Terry, M., Le, Q., et al. Program synthesis with large language models. *arXiv preprint arXiv:2108.07732*, 2021b.
- Bao, W., Chen, Z., Xu, D., and Shang, Y. Learning to parallel: Accelerating diffusion large language models via learnable parallel decoding. *arXiv preprint arXiv:2509.25188*, 2025.
- Ben-Hamu, H., Gat, I., Severo, D., Nolte, N., and Karrer, B. Accelerated sampling from masked diffusion models via entropy bounded unmasking. In *NeurIPS*, 2025.
- Campbell, A., Benton, J., De Bortoli, V., Rainforth, T., Deligiannidis, G., and Doucet, A. A continuous time framework for discrete denoising models. In *NeurIPS*, 2022.
- Chang, H., Zhang, H., Jiang, L., Liu, C., and Freeman, W. T. Maskgit: Masked generative image transformer. In *CVPR*, 2022.
- Chen, M., Tworek, J., Jun, H., Yuan, Q., Pinto, H. P. D. O., Kaplan, J., Edwards, H., Burda, Y., Joseph, N., Brockman, G., et al. Evaluating large language models trained on code. *arXiv preprint arXiv:2107.03374*, 2021.
- Chen, Z., Fang, G., Ma, X., Yu, R., and Wang, X. dparallel: Learnable parallel decoding for dllms. *arXiv preprint arXiv:2509.26488*, 2025.
- Cobbe, K., Kosaraju, V., Bavarian, M., Chen, M., Jun, H., Kaiser, L., Plappert, M., Tworek, J., Hilton, J., Nakano, R., et al. Training verifiers to solve math word problems. *arXiv preprint arXiv:2110.14168*, 2021.
- Gao, L., Tow, J., Abbasi, B., Biderman, S., Black, S., DiPofi, A., Foster, C., Golding, L., Hsu, J., Le Noac’h, A., Li, H., McDonnell, K., Muennighoff, N., Ociepa, C., Phang, J., Reynolds, L., Schoelkopf, H., Skowron, A., Sutawika, L., Tang, E., Thite, A., Wang, B., Wang, K., and Zou, A. The language model evaluation harness, 07 2024. URL <https://zenodo.org/records/12608602>.
- Hendrycks, D., Burns, C., Kadavath, S., Arora, A., Basart, S., Tang, E., Song, D., and Steinhardt, J. Measuring mathematical problem solving with the math dataset. In *NeurIPS Datasets and Benchmarks Track*, 2021.
- Ho, J., Jain, A., and Abbeel, P. Denoising diffusion probabilistic models. In *NeurIPS*, 2020.
- Hoogeboom, E., Nielsen, D., Jaini, P., Forré, P., and Welling, M. Argmax flows and multinomial diffusion: Learning categorical distributions. In *NeurIPS*, 2021.
- Israel, D., Broeck, G. V. d., and Grover, A. Accelerating diffusion llms via adaptive parallel decoding. In *NeurIPS 2025*, 2025.
- Jawahar, G., Sagot, B., and Seddah, D. What does bert learn about the structure of language? In *ACL*, 2019.
- Joshi, M., Choi, E., Weld, D. S., and Zettlemoyer, L. Triviaqa: A large scale distantly supervised challenge dataset for reading comprehension. *arXiv preprint arXiv:1705.03551*, 2017.
- Kang, W., Galim, K., Oh, S., Lee, M., Zeng, Y., Zhang, S., Hooper, C., Hu, Y., Koo, H. I., Cho, N. I., et al. Parallel-bench: Understanding the trade-offs of parallel decoding in diffusion llms. *arXiv preprint arXiv:2510.04767*, 2025.
- Khanna, S., Kharbanda, S., Li, S., Varma, H., Wang, E., Birnbaum, S., Luo, Z., Miraoui, Y., Palrecha, A., Ermon, S., et al. Mercury: Ultra-fast language models based on diffusion. *arXiv preprint arXiv:2506.17298*, 2025.
- Kim, B., Jeon, D., Kim, D., Jeung, W., and No, A. Rainbow padding: Mitigating early termination in instruction-tuned diffusion llms. *arXiv preprint arXiv:2510.03680*, 2025a.
- Kim, J., Shah, K., Kontonis, V., Kakade, S. M., and Chen, S. Train for the worst, plan for the best: Understanding token ordering in masked diffusions. In *ICML*, 2025b.
- Kim, S. H., Hong, S., Jung, H., Park, Y., and Yun, S.-Y. Klass: Kl-guided fast inference in masked diffusion models. In *NeurIPS*, 2025c.
- Koller, D. and Friedman, N. *Probabilistic graphical models: principles and techniques*. MIT press, 2009.
- Loshchilov, I. and Hutter, F. Decoupled weight decay regularization. *arXiv preprint arXiv:1711.05101*, 2017.
- Lou, A., Meng, C., and Ermon, S. Discrete diffusion modeling by estimating the ratios of the data distribution. In *ICML*, 2024.

- Nie, S., Zhu, F., You, Z., Zhang, X., Ou, J., Hu, J., Zhou, J., Lin, Y., Wen, J.-R., and Li, C. Large language diffusion models. In *NeurIPS*, 2025.
- Ou, J., Nie, S., Xue, K., Zhu, F., Sun, J., Li, Z., and Li, C. Your absorbing discrete diffusion secretly models the conditional distributions of clean data. In *ICLR*, 2025.
- Peebles, W. and Xie, S. Scalable diffusion models with transformers. In *ICCV*, 2023.
- Radford, A., Narasimhan, K., Salimans, T., and Sutskever, I. Improving language understanding by generative pre-training. *OpenAI Blog*, 2018.
- Radford, A., Wu, J., Child, R., Luan, D., Amodei, D., and Sutskever, I. Language models are unsupervised multitask learners. *OpenAI Blog*, 2019.
- Sahoo, S., Arriola, M., Schiff, Y., Gokaslan, A., Marroquin, E., Chiu, J., Rush, A., and Kuleshov, V. Simple and effective masked diffusion language models. In *NeurIPS*, 2024.
- Shi, J., Han, K., Wang, Z., Doucet, A., and Titsias, M. Simplified and generalized masked diffusion for discrete data. In *NeurIPS*, 2024.
- Sohl-Dickstein, J., Weiss, E., Maheswaranathan, N., and Ganguli, S. Deep unsupervised learning using nonequilibrium thermodynamics. In *ICML*, 2015.
- Song, J. and Zhou, L. Ideas in inference-time scaling can benefit generative pre-training algorithms. *arXiv preprint arXiv:2503.07154*, 2025.
- Song, Y. and Ermon, S. Generative modeling by estimating gradients of the data distribution. In *NeurIPS*, 2019.
- Song, Y., Sohl-Dickstein, J., Kingma, D. P., Kumar, A., Ermon, S., and Poole, B. Score-based generative modeling through stochastic differential equations. In *ICLR*, 2021.
- Tenney, I., Das, D., and Pavlick, E. Bert rediscovers the classical nlp pipeline. In *ACL*, 2019a.
- Tenney, I., Xia, P., Chen, B., Wang, A., Poliak, A., McCoy, R. T., Kim, N., Van Durme, B., Bowman, S. R., Das, D., et al. What do you learn from context? probing for sentence structure in contextualized word representations. In *ICLR*, 2019b.
- Welsh, D. J. and Powell, M. B. An upper bound for the chromatic number of a graph and its application to timetabling problems. *The Computer Journal*, 1967.
- Wu, C., Zhang, H., Xue, S., Liu, Z., Diao, S., Zhu, L., Luo, P., Han, S., and Xie, E. Fast-dllm: Training-free acceleration of diffusion llm by enabling kv cache and parallel decoding. *arXiv preprint arXiv:2505.22618*, 2025.
- Ye, J., Xie, Z., Zheng, L., Gao, J., Wu, Z., Jiang, X., Li, Z., and Kong, L. Dream 7b: Diffusion large language models. *arXiv preprint arXiv:2508.15487*, 2025.
- Zheng, L., Yuan, J., Yu, L., and Kong, L. A reparameterized discrete diffusion model for text generation. In *COLM*, 2024.
- Zhou, J., Lu, T., Mishra, S., Brahma, S., Basu, S., Luan, Y., Zhou, D., and Hou, L. Instruction-following evaluation for large language models. *arXiv preprint arXiv:2311.07911*, 2023.

A. Details of the Toy Experiments

Here, we provide additional details regarding the graph experiments discussed in Sec. 3.2. We employ the DiT (Peebles & Xie, 2023) architecture within the RADD (Ou et al., 2025) framework, configured with a total of eight transformer blocks. We train 30 masked diffusion models, each on a different dataset constructed according to the same MRF procedure (Sec. 3.2), for 20,000 gradient steps using the AdamW optimizer (Loshchilov & Hutter, 2017) with a learning rate of 10^{-3} . The training objective follows that of LLaDA (Nie et al., 2025).

Dependency scores s_{ij} are computed by averaging attention scores from the final two of the eight transformer blocks (25%). We empirically observe similar patterns when using attention from one, two, or three of the final blocks.

Evaluation details. When evaluating the validity of attention scores for MRF edge and degree estimation, we use step-by-step decoding. Out of the nine decoding steps, metrics are computed up to the seventh step, as beyond this point only a single edge connecting two nodes remains. All results are obtained by averaging metrics over 100 random sampling paths and across 30 independently trained models. See Tab. 3 for details.

Steps	Edge Detection		Degree Estimation
	AUC	Edge/Non-edge Attn. Ratio	OVR
1	0.923 ±0.00	2.19 ±0.00	0.00 ±0.00
2	0.923 ±0.02	2.21 ±0.12	0.04 ±0.01
3	0.919 ±0.04	2.18 ±0.23	0.05 ±0.01
4	0.916 ±0.04	2.17 ±0.21	0.08 ±0.02
5	0.937 ±0.05	2.23 ±0.24	0.05 ±0.01
6	0.937 ±0.10	2.17 ±0.37	0.04 ±0.02
7	0.944 ±0.12	2.28 ±0.45	0.02 ±0.04
8	—	—	—
9	—	—	—

Table 3. Edge detection and degree estimation metrics across decoding steps, reported as mean ± standard deviation over sampling paths.

Table 4. Accuracy (%) and average decoding steps (in parentheses) under single-block and four-block decoding. Compared to the four-block setting, all baselines exhibit substantially lower accuracy in the single-block regime due to EOS overflow (Kim et al., 2025a).

Method	Blocks	HumanEval	MBPP	GSM8K	Math500	IFEval
KLASS	1	10.98 (97.3)	19.80 (43.3)	26.31 (72.6)	3.00 (83.4)	40.05 (96.5)
	4	37.80 (149.4)	26.00 (53.9)	75.59 (93.9)	26.40 (118.6)	58.39 (139.0)
Fast-dLLM	1	10.37 (40.7)	9.60 (34.2)	7.51 (89.4)	1.80 (76.4)	41.73 (31.7)
	4	37.20 (92.1)	20.60 (41.5)	76.80 (72.8)	28.00 (95.6)	58.27 (100.0)
EB-Sampler	1	13.41 (85.9)	8.00 (61.1)	6.60 (143.4)	2.00 (136.3)	30.70 (108.3)
	4	37.20 (112.1)	19.40 (52.6)	76.12 (86.9)	28.20 (113.2)	56.95 (136.3)

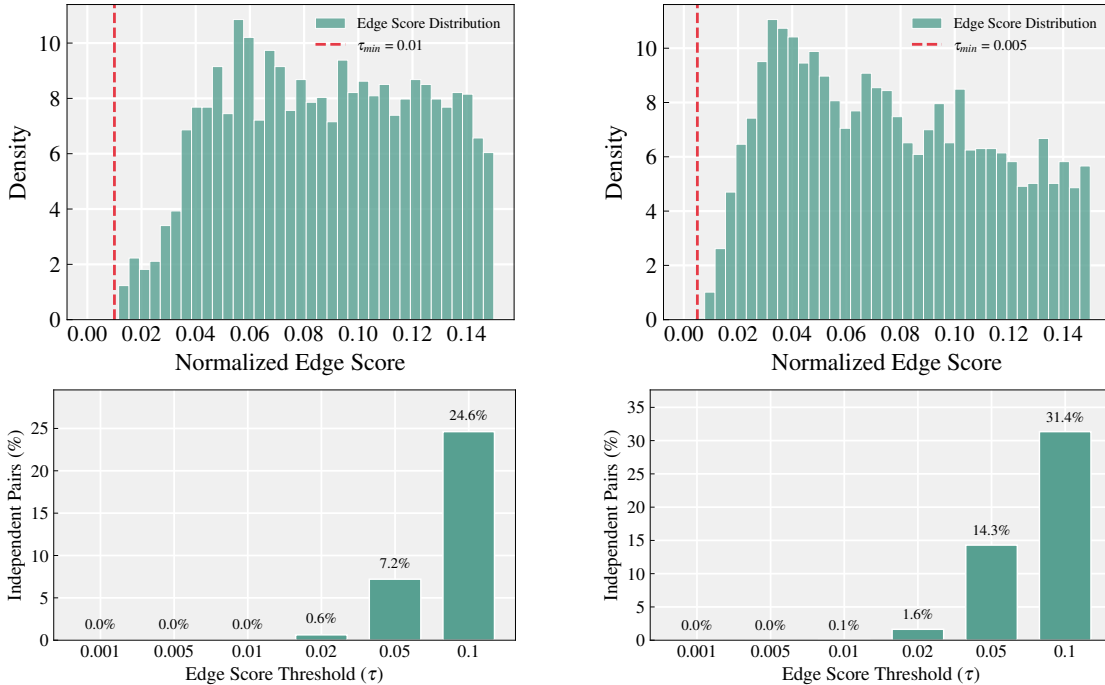


Figure 6. Analysis of τ_{min} . Left: LLaDA. Right: Dream.

B. Details on Main Experiments

Basic setup. All experiments are conducted on NVIDIA L40S GPUs. For consistent and reproducible evaluation, we disable stochastic decoding parameters such as temperature. We use the `lm-eval` framework for all evaluations, following its default setting for the number of few-shot examples. These settings are applied consistently across both LLaDA and Dream. For LLaDA, we additionally report results under both single-block and four-block decoding for the training-free baselines. As shown in Tab. 4, baselines suffer severe performance degradation in the 1-block decoding due to premature termination from *EOS overflow* (Kim et al., 2025a), whereas four-block decoding substantially mitigates this issue.

Hyperparameter details. For commonly used benchmarks (HumanEval, MBPP, Math500, GSM8K), we adopt the best hyperparameter settings for baseline methods (EB-Sampler, KLASS, Fast-dLLM) as reported in their original papers or official code implementations. We refer readers to the respective works for detailed configurations. As there are no established hyperparameter references for the IFEval task, we perform hyperparameter sweeps for each baseline method. For EB-Sampler, we vary the parameter γ over $\{0.05, 0.1, 0.15, 0.2\}$ for LLaDA and Dream. For Fast-dLLM and KLASS, we sweep the confidence threshold over $\{0.8, 0.85, 0.9, 0.95\}$. For KLASS, we sweep the KL threshold over $\{0.001, 0.005\}$ for both LLaDA and Dream. After sweeping, we select the configuration that achieves the most favorable trade-off between accuracy and steps, and report those results in the main section.

For DAPD, we use a hyperparameter τ_t to determine whether a token is selected for sampling based on its attention-based edge score. We adopt a simple linear schedule in which τ_t increases over the decoding process. For LLaDA, we use a linear τ_t schedule over $[0.01, 0.05]$ for math tasks (Math500, GSM8K) and $[0.01, 0.15]$ for all remaining tasks. For Dream, we use a linear τ_t schedule over $[0.005, 0.05]$ across all tasks; for IFEval, we use $[0.1, 0.5]$. To motivate our choice of τ_{min} , we empirically characterize the distribution of *normalized mask-to-mask edge scores* under the Sec. 6 analysis setup. Specifically, for both LLaDA and Dream with generation length 256, we run decoding step-by-step and, at each step, collect pairwise edge scores among the remaining masked positions. As shown in Fig. 6, we observe that the chosen values, $\tau_{min} = 0.01$ for LLaDA and $\tau_{min} = 0.005$ for Dream, fall in the near-zero tail of the observed edge score distribution, so the early-stage decoding admits only very weak interactions between concurrently updated positions. In practice, decreasing τ_{min} further has little effect on the available set of low-dependency pairs, as the fraction of pairs below such small thresholds remains close to zero in our measurements.

Details on ParallelBench. We additionally run ParallelBench (Kang et al., 2025), a benchmark designed to assess parallel decoding capability, using its native evaluation protocol. ParallelBench comprises multiple task types with task-specific generation lengths and instance sizes. Across tasks, n denotes the task-specific problem size (instance size), e.g., the number of entities in *waiting line*, the grid/order in *Latin square* (and related puzzle settings), or a difficulty parameter in *words to sentence*. We evaluate the following task types and subtasks: **Waiting Line** ($n = 15$) (10 subtasks; generation length = 128; we use the $n=15$ variant rather than the default waiting line since the latter uses generation length = 32, which is less suitable for evaluating parallel decoding): copy, insert (index), insert (random), remove (index), remove (random), replace (index), replace (random), reverse, shuffle, sort. **Puzzle** (2 subtasks; generation length = 64): Latin square ($n = 4$), Sudoku ($n = 4$, 12 clues). **Paraphrase and Summarize** (2 subtasks; generation length = 128): ChatGPT paraphrase, SAMSum summarization. **Words to Sentence** (6 subtasks; generation length = 64): easy, easy ($n = 1$), easy ($n = 3$), easy ($n = 4$), easy ($n = 5$), easy ($n = 6$).

For our method, we use a single shared schedule $\tau_t \in [0.001, 0.005]$ for all ParallelBench task types. For training-free baselines, we use their default hyperparameters under the LLaDA setup: Fast-dLLM uses confidence threshold 0.9; EB-Sampler uses $\gamma = 0.1$; KLASS uses confidence threshold 0.9 and KL threshold 0.001. All other settings follow the official ParallelBench protocol.

C. Details on Analysis

Here we provide details of the experimental setup for Sec. 6, which examines the decoding behavior of various parallel decoding strategies on independently aggregated queries.

Dataset construction. We curate the dataset by sampling from TriviaQA (Joshi et al., 2017). We filter out lengthy or ambiguous questions to retain simple, common-knowledge queries with concise answers.

To ensure high-quality factual recall, we applied several structural and semantic filters to the curated subset. All questions were required to terminate with a question mark or initiate with standard interrogative tokens (e.g., What, Which, Who, Where, When). We restricted queries to a single sentence with a maximum length of 120 characters. Furthermore, we mitigated ambiguity by explicitly excluding questions containing comparative or restrictive phrases—such as “which of the following,” “best describes,” or “most likely”—thereby ensuring a mapping to singular ground-truth entities. Finally, we removed questions beginning with “Why” or “How”, as these typically necessitate complex generative explanations rather than the direct, noun-centric factual recall targeted in this study.

Below are examples of the filtered questions:

- *What is the name of the parson mentioned in the lyrics of the Christmas carol “Winter Wonderland”?*
- *Who played ‘Peter Pan’ in Spielberg’s ‘Hook’?*
- *Who won the Formula 1 World Championship in 1992?*
- *Who wrote, produced and directed epic film, Avatar?*

After filtering, we obtain a total of 12,380 questions. We then randomly sample five independent questions and aggregate them into a single instance, constructing 500 samples in total (2,500 individual questions). To encourage explicit reasoning, we include instructions and illustrative examples that require the model to explain its reasoning rather than output only final answers. The prompt template is shown below.

Please answer the following 5 independent questions.

Instructions:

- 1) Write answers in full sentence format.
- 2) Explain your reasoning step by step before stating the final answer.
- 3) Write the final answer after "Therefore, the answer is".
- 4) Keep the numbering format [1], [2], [3], [4], [5].

Here are examples showing how your answers should be written:

[Example 1]

Question: What is the smallest country in the world by area?

Answer: To determine the smallest country, we compare the land areas of sovereign states. Although countries like Monaco and San Marino are very small, Vatican City has an area of about 0.44 square kilometers, which is smaller than any other country. Therefore, the answer is Vatican City.

[Example 2]

Question: How many continents are there on Earth?

Answer: Continents are large continuous landmasses. These include Africa, Antarctica, Asia, Europe, North America, South America, and Australia. Counting these gives a total of seven continents. Therefore, the answer is seven.

Now answer the following questions in the same style:

- [1] {Question 1}
- [2] {Question 2}
- [3] {Question 3}
- [4] {Question 4}
- [5] {Question 5}

Evaluation details. We evaluate accuracy by string matching against ground truth answers and aliases in the model outputs. For each prompt instance, which contains five independent questions, we first extract the corresponding answer segment using the bracketed markers [1], [2], etc. We then identify the predicted answer by parsing the text following the canonical phrase “Therefore, the answer is” (or the fallback “The answer is”) and perform case-insensitive substring matching against the ground truth answer and its alias set. If no such phrase is detected, we fall back to matching over the entire generated segment. We report accuracy as the fraction of questions for which the answer (or an alias) is matched, aggregated over all questions in the dataset. In addition, we report the average number of function evaluations (NFE) as a measure of decoding steps (Tab. 2), computed by averaging the per-sample NFE values in each method’s output file.

Hyperparameter details. All experiments are conducted using LLaDA. We sweep several hyperparameters for each baseline. For EB-Sampler, we vary the parameter γ over $\{0.05, 0.1, 0.15, 0.2\}$, while for Fast-dLLM and KLASS, we sweep the confidence threshold over $\{0.6, 0.7, 0.8, 0.9\}$. For KLASS, we sweep the KL threshold over $\{0.001, 0.0015, 0.015, 0.1, 0.2\}$. We report results for each baseline using the hyperparameter setting that yields the highest accuracy. For DAPD, we apply a linear τ_t schedule over $[0.01, 0.05]$, consistent with the default configuration used in our LLaDA experiments.

D. Additional Qualitative Results on Analysis

Visualizations of the unmasking trajectories for EB-Sampler and KLASS (corresponding to the analysis in Fig. 1) are provided in Figs. 9 and 11, respectively.

This section is organized by method for ease of comparison: DAPD (Figs. 7 and 8), EB-Sampler (Figs. 9 and 10), KLASS (Figs. 11 and 12), and Fast-dLLM (Figs. 13 and 14).

